Journal of Environmental Chemical Engineering 10 (2022) 107874

Contents lists available at ScienceDirect

Journal of Environmental Chemical Engineering

journal homepage: www.elsevier.com/locate/jece

Reinforced degradation of ibuprofen with $MnCo_2O_4$/FCNTs nanocatalyst as peroxymonosulfate activator: Performance and mechanism

Chao He [a,*], Chunyan Tang [b], Wen-Da Oh [c,*]

[a] Faculty of Engineering and Natural Sciences, Tampere University, Tampere, Finland
[b] Key Laboratory of Integrated Regulation and Resource Development on Shallow Lake of Ministry of Education, College of Environment, Hohai University, Nanjing 210098, China
[c] School of Chemical Sciences, Universiti Sains Malaysia, 11800 Penang, Malaysia

ARTICLE INFO

Editor: Teik Thye Lim

Keywords:
Peroxymonosulfate
$MnCo_2O_4$
Functionalized carbon nanotubes
Sulfate radicals
Catalytic mechanism

ABSTRACT

In order to efficiently degrade ibuprofen (IBU) by peroxymonosulfate (PMS) activation, manganese cobalt oxide nanoparticles-decorated functionalized multi-walled carbon nanotubes ($MnCo_2O_4$/FCNTs) were prepared using a facile hydrothermal method. Comprehensive characterization of this PMS activator in multi-scale suggested that $MnCo_2O_4$ nanoparticles were uniformly decorated on FCNTs. The catalytic performance was systematical evaluated under various environmental conditions, including temperature, pH, and the presence of different common water matrix species (e.g., Cl^-, HCO_3^-, and natural organic matter). The as-synthesized $MnCo_2O_4$/FCNTs demonstrated excellent catalytic activity with k_{app} ranging 0.285–0.327 min^{-1} under a wide pH range of 3–9 within 10 min, which achieved a complete removal of IBU and a mineralization rate higher than 90%. During oxidation process for stability and reusability test, recycled $MnCo_2O_4$/FCNTs was found durable with negligible leaching of metal ions from spent catalyst, exhibiting its high stability for PMS activation with merely slight decrease of k_{app} from 0.285 to 0.201 min^{-1} in the fourth cycle. Electron paramagnetic resonance analysis further confirmed that $^{\bullet}OH$, $SO_4^{\bullet-}$ and $^1O_2$ were generated in the robust $MnCo_2O_4$/FCNTs-PMS system. Both radical and nonradical reactions were found to be responsible for the enhanced IBU degradation. Overall, this study sheds light on practical knowledge of IBU removal using $MnCo_2O_4$/FCNTs for PMS activation.

1. Introduction

Pharmaceutical and personal care products (PPCPs) are currently released into the aquatic environment through multiple pathways, including domestic wastewater, hospital discharge, improper manufacturing disposal, effluents from water treatment plants (WTPs) and sewage treatment plants (STPs) [1,2]. PPCPs could cause endocrine disruption and chronic toxicity to human health and aquatic microorganisms [3]. Because of their resistance to biodegradation during conventional activated sludge process in STPs, the occurrence of PPCPs in receiving waterbody becomes an emerging concern [4,5]. Thus, it is imperative to develop a more effective technique for degradation of PPCPs.

Advanced oxidation processes (AOPs) have been widely regarded as an efficient technique for degradation of recalcitrant organic contaminants in water environment. Especially, sulfate radical ($SO_4^{\bullet-}$) based AOPs have attracted great interest in the abatement of micro-pollutants in water treatment [6,7]. $SO_4^{\bullet-}$ has become an alternative to hydroxyl radical ($^{\bullet}OH$) due to a relatively higher redox potential of 2.5–3.1 V. As a strong one-electron oxidant, $SO_4^{\bullet-}$ can readily react by addition to C-C double bonds and by H-abstraction [8]. Besides, $SO_4^{\bullet-}$ exhibits other obvious advantages over $^{\bullet}OH$ in terms of wider application pH range of 2–8 and longer lifespan of 30–40 μs [9–11]. In particular, PMS is a cost-effective and environmentally friendly oxidant with lower energy input and alkaline dosing [12]. Currently, cobalt (Co) is considered the most effective transition metal catalyst for PMS activation [13]. However, Co^{2+} in aqueous solution leads to further environmental pollution and health issues. Recently, Mn oxide [14–16] and supported Mn oxide catalysts [17,18] have demonstrated excellent catalytic activity as PMS activator for degradation of organic pollutants. Thus, it is of great interest to develop novel and efficient Mn oxide catalysts with less environmental toxicity to activate PMS for the decomposition of emerging PPCPs.

In the last decade, spinel ferrite nanoparticles with a general

* Corresponding authors.
E-mail addresses: chao.he@tuni.fi (C. He), ohwenda@usm.my (W.-D. Oh).

https://doi.org/10.1016/j.jece.2022.107874
Received 9 March 2022; Received in revised form 3 May 2022; Accepted 6 May 2022
Available online 10 May 2022

formula, MCo_2O_4 (M = Mn, Fe, Co, Ni or Cu), have been used in several applications such as catalysis, environmental remediation, and supercapacitor, due to their outstanding properties in terms of nanometer size, large surface area to volume ratio, and superparamagnetic behavior [11,19,20]. As PMS activator, $Co_xMn_{3-x}O_4$ [21] and $MnFe_2O_4$ [22] were found to be active for oxidation of organic pollutants. Despite high catalytic activity of $MnCo_2O_4$ nanoparticles (NPs), NPs materials could result in lower catalytic efficiency as a result of aggregation, lower electrical conductivity, poor electron transfer rate, and limited active sites. To solve these issues, carbonaceous materials with high electrical conductivity and buffer matrix can br employed as matrices for $MnFe_2O_4$-based materials to provide a larger surface area for the diffusion of reactants onto the active sites, thereby enhancing their catalytic performance.

As compared to other carbon materials (e.g., graphene, activated carbon, or graphite), carbon nanotubes (CNTs) possess unique properties, such as large surface area, high stability and mechanical strength, making CNTs suitable as support materials of various catalysts [23–25]. The advantages of spontaneous redox reactions between CNTs and metal oxides have been recognized earlier [26]. The excellent electrical conductivity of CNTs could not only help to stabilize the active intermediates but also facilitate the catalytic processes involving electron transfer. Meanwhile, CNT-$CoFe_2O_4$ @PPy has been used as adsorbent and catalyst to remove anionic and cationic dyes [23]. Meanwhile, the stability of the PMS activator is also of critical importance in order to prepare eco-friendly nanoparticles or catalysts for practical application, thus the leaching of metal ions from the PMS activator should be substantially hindered. However, to the best of our knowledge, there is no literature on the exploration of robust and stable $MnCo_2O_4$ supported on functionalized CNTs ($MnCo_2O_4$/FCNTs) for PMS activation in degradation of organic contaminants.

In the present work, we report a facile approach to prepare $MnCo_2O_4$/FCNTs and its catalytic activation in PMS oxidation of ibuprofen (IBU). The properties of $MnCo_2O_4$/FCNTs and its catalytic performance were investigated in terms of effects of various reaction parameters (e.g., pH, temperature, Cl^-, HCO_3^- and natural organic matter (NOM)) on IBU removal. Furthermore, PMS activation mechanism and the dominant reactive oxygen species (ROS) were evaluated.

2. Experimental

2.1. Chemicals and materials

Commercial multi-walled CNTs (> 97%) were obtained from Shenzhen Nanotech Port Co., Ltd. Ibuprofen (IBU, ≥98%), oxone ($2KHSO_5{\cdot}KHSO_4{\cdot}K_2SO_4$, PMS), cobalt nitrate hexahydrate ($Co(NO_3)_2.6\ H_2O$, AR, 99%), manganese nitrate solution ($Mn(NO_3)_2.6\ H_2O$, AR, 50 wt%), sodium bicarbonate , sodium chloride , humic acid, 5,5-dimethyl-1-pyrroline N-oxide (DMPO, >99.0%), and 4-oxo-2,2,6,6-tetramethyl-4-piperidone (TEMP, >99.0%) were purchased from Aladdin Chemistry Co., Ltd. (Shanghai, China). Sodium hydroxide, sulfuric acid and ethyl alcohol were obtained from Chemical Reagents (Guangzhou, China). All these reagents were used without any further purification. Deionized water (18.25 MΩ·cm) used in all the experiments was prepared by an ultrapure water purification system (Ulupure, China).

2.2. Preparation of catalysts

CNTs were employed as support materials for bimetallic catalysts preparation. Pristine CNTs were refluxed in concentrated nitric acid at 120 °C for 4 h under stirring to remove metallic impurities and introduce oxygen-containing functional groups onto the surface of CNTs, thereby facilitating uniform precipitation of metal precursors [27]. The functionalized CNTs were washed and prepared following the procedure described by Nassr et al. [28], which were denoted as FCNTs thereafter. All monometallic and bimetallic nanomaterials were prepared using a hydrothermal method. Specifically, 0.218 g $Co(NO_3)_2.6\ H_2O$, 0.0134 g $Mn(NO_3)_2.6\ H_2O$ and 25 mg FCNTs were added into a round bottomed flask with 37.5 mL ethyl alcohol. The mixture was vigorously mixed in a rotary vibrator at 300 rpm for 12 h under room temperature. The suspension was then dispersed by ultrasound for 1 h followed by filtration and washing with deionized water and acetone. This composite was subsequently transferred into a 100 mL Teflon-lined stainless-steel autoclave for hydrothermal reaction at 140 °C for 12 h. The autoclave was naturally cooled down to room temperature afterwards. The formed composite was vacuum dried at 60 °C for 12 h and was then calcined at 500 °C for 2 h under vacuum. The as-synthesized catalyst was denoted as $MnCo_2O_4$/FCNTs.

2.3. Catalyst characterizations

X-ray diffraction (XRD) patterns were obtained on a Bruker D8 diffractometer (Bruker-AXS, Karlsruhe, Germany) using Cu-Kα radiation X-ray source (λ = 1.5418 Å) operated at 40 kV and 26 mA. The data were collected with a 2θ ranging from 10° to 90° at a step width of 0.02°. Specific surface area and pore size distribution were determined through nitrogen adsorption/desorption at − 196 °C on a Micromeritics Tristar II 3020 system using multi-point Brunauer-Emmett-Teller (BET) method. Prior to measurements, the catalysts were degassed at 150 °C for 12 h under vacuum. Surface morphology of as-synthesized $MnCo_2O_4$/FCNTs was examined by scanning electron microscopy (SEM) (ZEISS Gemini 500) with an acceleration voltage of 10 kV. Nanoscale structure was observed using high resolution transmission electron microcopy (HRTEM) (JEOL JEM-2100 F) with an acceleration voltage of 200 kV. X-ray photoelectron spectroscopy (XPS) spectra analysis was carried out on a Thermo Fisher Scientific ESCALAB 250 electron spectrometer with a monochromatic Al Kα X-ray radiation source ($h\nu$ = 1486.6 eV).

2.4. Catalytic oxidation of IBU

Pharmaceutical wastewater containing high concentration of IBU has been simulated. Catalytic oxidation experiments were conducted in a 250 mL batch reactor at 25.0 ± 0.2 °C and 300 rpm in a water bath shaker. According to previous study system [29], initial IBU concentration of 10 mg/L was applied and solution pH was adjusted by 0.1 M HNO_3 and 0.1 M NaOH. The dosage of PMS and $MnCo_2O_4$/FCNTs was 1.0 g/L and 0.01 g/L, respectively. During the oxidation process, 1 mL of IBU solution was sampled at a pre-determined interval and quenched quickly with 0.1 mL methanol followed by filtration using 0.22 μm cellulose acetate membrane for further analysis. Meanwhile, non-catalytic control experiments were carried out under identical conditions. Catalytic stability of $MnCo_2O_4$/FCNTs was examined through recycling test. Specifically, solid catalysts were filtered and recycled using 0.22 μm Millipore filter and washed with deionized water followed by vacuum drying at 60 °C for 12 h before reuse.

2.5. Analytical and evaluation methodologies

The concentration of IBU with an injection volume of 10 μl was determined at 223 nm by a high performance liquid chromatography (HPLC) (Shimadzu Essentia LC-16) system equipped with a UV-Vis detector (SPD-16). The separation was performed on a WondaSil C18-W*R* column (150 × 4.6 mm, 5 μm) using a pH of 2.1 mobile phase consisting of 80/20 (v/v) MeOH-H_2O binary solution at a flow rate of 1.0 mL/min and 30 °C. Electron paramagnetic resonance (EPR) spectra were measured on a Bruker A300–10/12 spectrometer using 5,5-dimethyl-1-pyrroline N-oxide (DMPO) and 4-oxo-2,2,6,6-tetramethyl-4-piperidone (TEMP) as spin-trapping agents. Total organic carbon (TOC) concentration in the reaction solution was analyzed using a TOC analyzer (Shimadzu TOC-VCPH) after filtration through 0.22 μm polytetrafluoroethylene (PTFE) syringe filter. Leaching of Mn and Co ions into reaction solution was detected using inductively coupled plasma optical

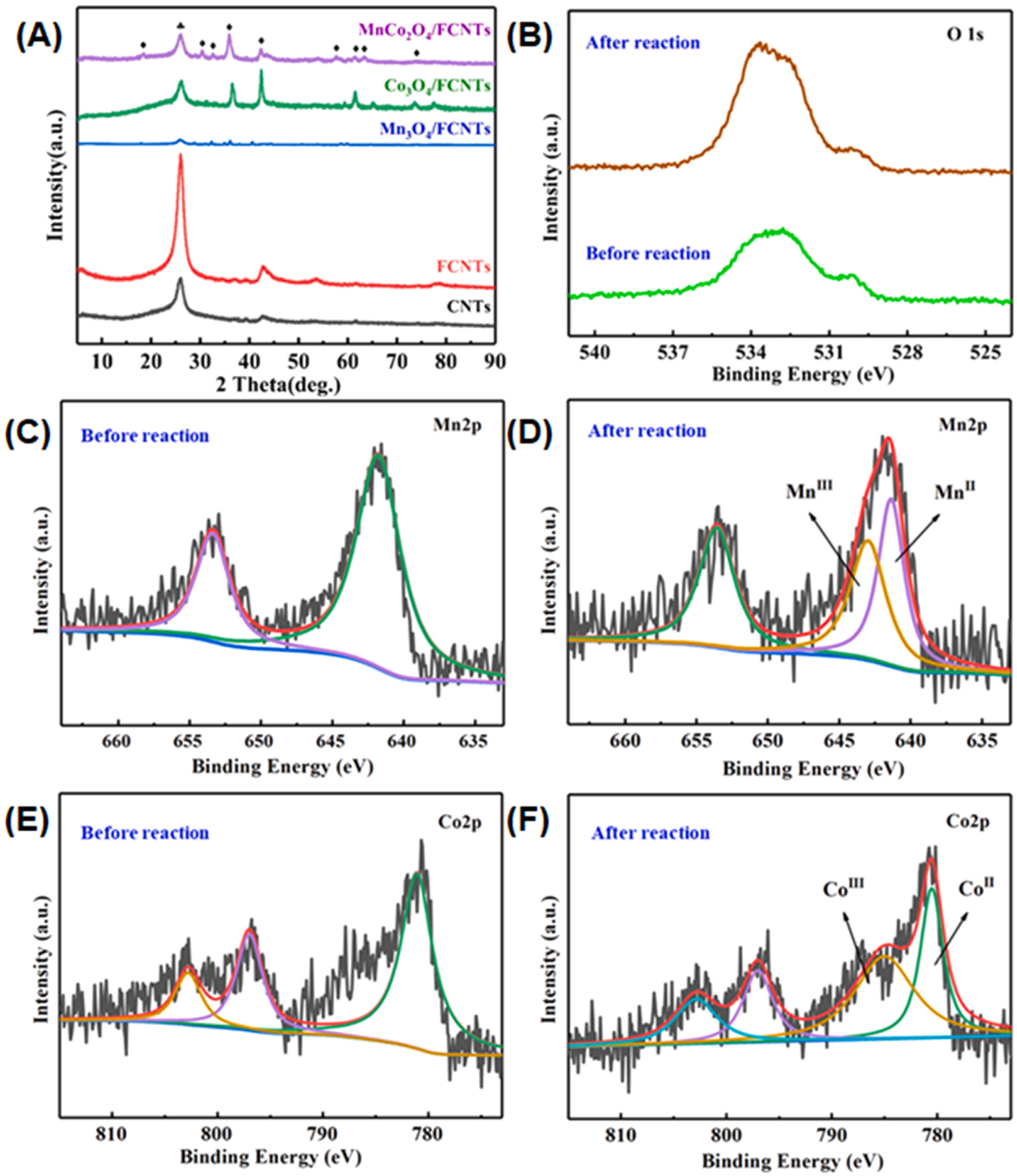

Fig. 1. (A) X-ray diffraction patterns of CNTs, FCNTs, and as-synthesized catalysts, and XPS spectra of the fresh and spent $MnCo_2O_4$/FCNTs: (B) O 1 s; (C) and (D) for Mn 2p; (E) and (F) for Co 2p.

emission spectrometry (ICP-OES) (PerkinElmer Optima 5300DV).

3. Results and discussion

3.1. Structural and physicochemical properties of catalysts

The XRD patterns of pristine CNTs, FCNTs, Mn_3O_4/FCNT, Co_3O_4/FCNT and $MnCo_2O_4$/FCNTs are depicted in Fig. 1**A**. A higher intensity of the diffraction peak at 25.9° for FCNTs implied the removal of impurities from pristine CNTs. The presence of a sharp XRD diffraction peak (002) of hexagonal graphite at 25.9° in all the catalysts indicated that the CNTs graphitic structure was retained after sequential HNO_3 oxidation, bimetallic impregnation, and high temperature reduction processes. Meanwhile, several well-defined peaks at 19.3°, 26.5°, 30.9°, 33.6°,

Table 1
XPS analysis of surface elements of CNTs, FCNTs, $MnCo_2O_4$/FCNTs, and spent $MnCo_2O_4$/FCNTs.

Catalysts	C 1 s (wt %)	O 1 s (wt %)	N 1 s (wt%)	Co 2p3 (wt%)	Mn 2p3 (wt%)
CNTs	89.27	9.21	1.52	–	–
FCNTs	87.75	12.25	–	–	–
$MnCo_2O_4$/FCNTs	89.27	10.01	0.11	0.38	0.23
Spent $MnCo_2O_4$/FCNTs	90.21	9.10	0.13	0.36	0.20

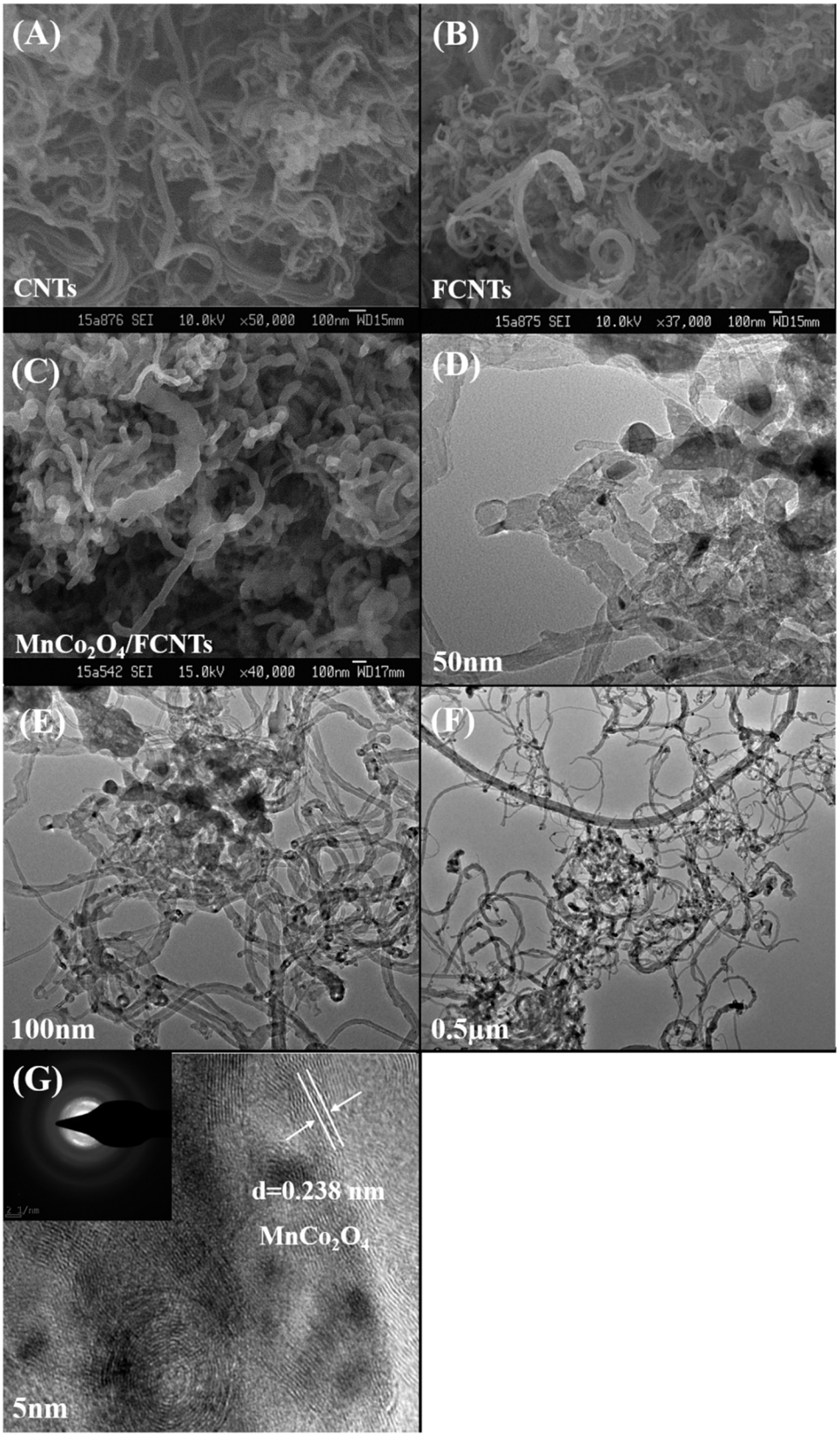

Fig. 2. SEM images of (A) pristine CNTs; (B) FCNTs; (C) $MnCo_2O_4$/FCNTs; HRTEM images (D, E, F and G) of $MnCo_2O_4$/FCNTs.

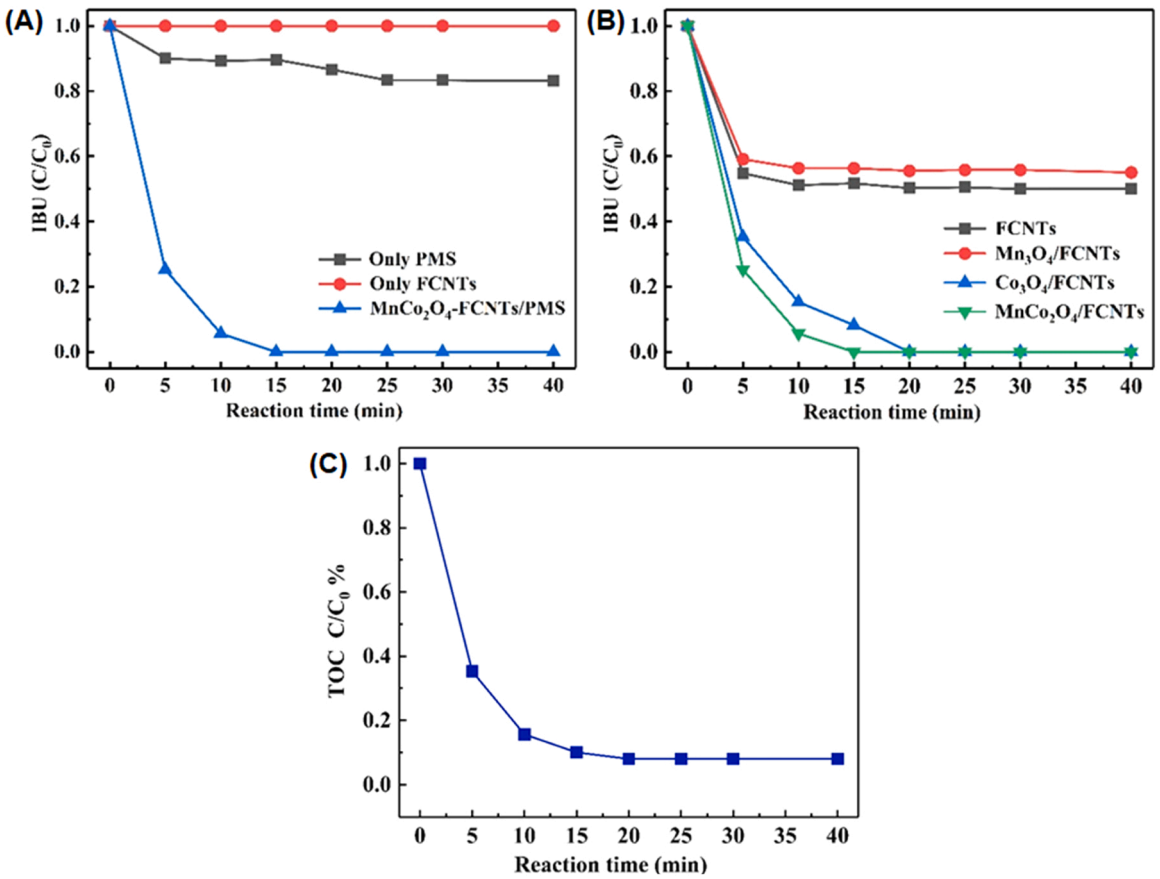

Fig. 3. (A – B) IBU degradation performance using different catalytic oxidation systems (B: All reactions are conducted in the PMS system), and (C) residual TOC in $MnCo_2O_4$/FCNTs-PMS system. Experimental conditions: $[IBU]_0 = 10$ mg/L; catalyst dosage = 0.1 g/L; $[PMS]_0 = 0.01$ g/L; $[pH]_0 = 4.7$; T = 25 °C.

36.4°, 43.1°, 57.9°, 62.1° and 74.8° can be indexed to (220), (311), (222), (400), (422), (511), (440), (622) and (553) reflection planes, respectively, for cubic-phase $MnCo_2O_4$ structure (JCPDS No. 75–1090). These peaks were also observed for $MnCo_2O_4$/FCNTs, indicating that crystalline $MnCo_2O_4$ nanoparticles were successfully immobilized onto FCNTs structure.

Chemical elements in the catalyst were analyzed using XPS technique and presented in Table 1 and Fig. 1**B-F**. As compared with the pristine CNTs, the high-resolution O 1 s spectra of FCNTs in Fig. 1**B** suggested that the oxygen content increased significantly from 9% to 12% after nitric acid reflux. The nitric acid oxidation of carbon materials induced formation of oxygen-containing groups (Fig. S1), including carboxylic acid, lactone, anhydride, quinone and hydroxyl groups, which are mainly attached to the defective edges of CNTs [28,30]. These functional groups could (i) facilitate the formation of the conduct network for increased electron transfer process during catalysis [31,32], (ii) anchor $MnCo_2O_4$ to increase the stability of the catalyst through stronger support-$MnCo_2O_4$ interaction [27], (iii) improve the dispersion of catalyst on CNTs, and (iv) enhance the mechanical properties of catalyst.

The EDS analysis was then performed to analyze the elemental distribution on the surface of $MnCo_2O_4$/FCNTs and the results indicated the presence of C, N, O, Mn, and Co. The morphology and structure of pristine CNTs, FCNTs and $MnCo_2O_4$/FCNTs were further investigated by SEM and HR-TEM. Fig. 2 shows that the diameter of $MnCo_2O_4$ particle was ranging from 100 to 200 nm with an average particle size of 63.5 nm. The relatively small particle size promoted higher specific surface area which was beneficial to improve the catalytic activity of $MnCo_2O_4$/FCNTs. Fig. 2**G** clearly shows a lattice distance of 0.238 nm that could be assigned to the dominant and exposed (311), (511), (553) and (555) planes of $MnCo_2O_4$ in the $MnCo_2O_4$/FCNTs catalyst, which is in good agreement with the XRD results. In Table S1, the specific surface area (S_{BET}) of CNTs and FCNTs was 178.0 and 204.5 m^2/g, respectively. After loading $MnCo_2O_4$, the S_{BET} was decreased to 112.3 m^2/g due to the formation of $MnCo_2O_4$ nanoparticles on FCNTs surface. This also shows the successful incorporation of $MnCo_2O_4$ onto the FCNTs framework. These physicochemical properties may contribute to different catalytic activities of these catalysts as discussed below.

3.2. Catalytic oxidation of IBU with PMS on $MnCo_2O_4$/FCNTs

Fig. 3 depicts the catalytic oxidation efficiencies of different catalysts for IBU removal under identical experimental condition. The results are fitted using a first-order kinetics$[IBU] = [IBU]_0 e^{-k_{app}t}$, where k_{app} is the apparent first-order rate constant. Specifically, all fittings were conducted using Microsoft Excel and gave a correlation coefficient (R^2) ranging from 0.9434 to 0.9987. In the control experiment with the absence of PMS, FCNTs alone showed no significant IBU adsorption (less than 2% of IBU removal efficiency) within 40 min in spite of a relatively large S_{BET} and porosity. On the other hand, in the absence of catalyst, PMS alone could hardly degrade IBU in the aqueous solution. In PMS system, $MnCo_2O_4$/FCNTs exhibited a high catalytic performance and a complete IBU removal was achieved within 10 min with k_{app} of 0.285 min^{-1}. The degradation rate of $MnCo_2O_4$/FCNTs was 2.62 and 1.53-fold of that for Mn_3O_4/FCNTs and Co_3O_4/FCNTs, respectively. In the first 5 min of the reaction, the rate constant of FCNTs, Mn_3O_4/FCNTs and Co_3O_4/FCNTs was 0.078, 0.067 and 0.192 min^{-1}, respectively. Apparently, synergy of FCNTs and $MnCo_2O_4$ could increase the catalytic activity through enhanced electron transfer efficiency and improved $MnCo_2O_4$ stability and dispersion. Thus, more effective PMS activation

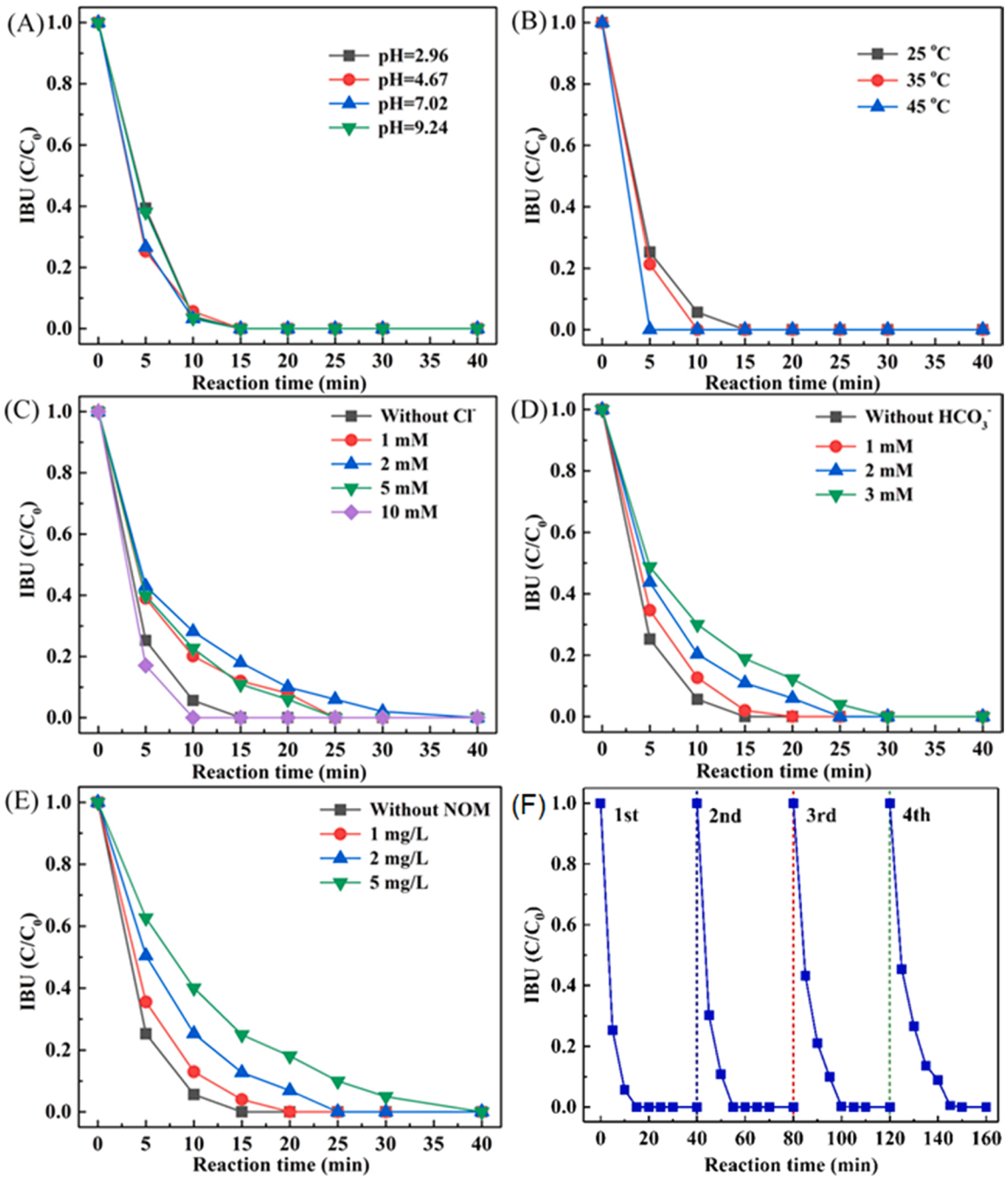

Fig. 4. Effects of different reaction conditions (A: pH; B: Temperature; C: Cl^-; D: HCO_3^-; E: NOM; F: Reusability) on the IBU degradation in $MnCo_2O_4$/FCNTs-PMS system. Experimental conditions: $[IBU]_0 = 10$ mg/L; catalyst dosage = 0.1 g/L; $[PMS]_0 = 0.01$ g/L; $[pH]_0 = 4.7$; T = 25 °C.

process could generate reactive oxygen species (ROS) with superior efficiency for IBU degradation. Comparison of the k_{app} of $MnCo_2O_4$/FCNTs (0.285 min^{-1}) [33] with other catalysts, such as Co_3O_4-rGO (0.117 min^{-1}) and C-ZnFe LDH (0.0184 min^{-1}) [34], for IBU degradation suggested that the as-synthesized $MnCo_2O_4$/FCNTs was more advantageous as it exhibited higher catalytic efficiency. Fig. 3C depicts the residual TOC after catalytic IBU degradation in the $MnCo_2O_4$/FCNTs-PMS system. The TOC gradually decreased to 0.9 mg/L, suggesting that IBU was almost completely mineralized with a mineralization rate higher than 90%. These results further confirm that $MnCo_2O_4$/FCNTs can effectively activate PMS to produce active species with high oxidation potential for IBU removal.

3.3. Influences of various reaction parameters

3.3.1. Effect of pH

The IBU degradation at different pH values in the $MnCo_2O_4$/FCNTs-PMS system is shown in Fig. 4A. On the whole, the IBU degradation in the $MnCo_2O_4$/FCNTs-PMS system under a wide pH range of 2.96–9.24 was generally lower than that within a relatively narrower pH range of 4.67–7.02. Considering the pKa value for IBU and PMS are 4.91 [35] and 9.4 [36], respectively, the point of zero charge of $MnCo_2O_4$/FCNTs is within the range of 4.9 ± 1.8 [37]. Thus, at pH 9.4, the electrostatic repulsion between the negatively charged PMS, IBU and $MnCo_2O_4$/FCNTs-PMS could be prominent, thereby inhibiting the overall IBU degradation rate. Similarly, at pH 2.96, the IBU degradation

rate was also inhibited, which could be ascribed to the scavenging effect of H^+ ion on the generated ROS [38]. Nevertheless, under pH 3–9, k_{app} ranged from 0.285 to 0.327 min^{-1}. This reveals that $MnCo_2O_4$/FCNTs may activate PMS at a satisfactory level within a wide pH range without distinctly losing its catalytic activity, which is in accordance with previous research results [32].

3.3.2. Effect of temperature

The degradation reaction of IBU was also significantly influenced by the reaction temperature. Generally, IBU removal would be promoted under increased reaction temperature. As shown in Fig. 4**B**, the degradation rate constant increased proportionally with increasing temperature from 25 to 45 °C. The k_{app} values were fitted with the Arrhenius equation (i.e., lnk_{app} versus 1/T) and the calculated activation energy was 2.6 kJ mol^{-1}. This activation energy was relatively lower than those in previous research using Mn-based catalysts [39,40], indicating that this as-synthesized catalyst could efficiently activate PMS. Previous research showed that elevating the reaction temperature may not only enhance the chemisorption of organic/PMS but also facilitate the electron-transfer process between pollutants and PMS via the carbon catalyst [41]. Therefore, the enhanced contribution of radicals in the $MnCo_2O_4$/FCNTs-PMS system could be attributed to generation of $SO_4^{\bullet-}$ and $^{\bullet}OH$ via the activation of PMS [32,41,42].

3.3.3. Effect of Cl^-

The effect of the presence of typical ions (e.g., Cl^-, HCO_3^-) on IBU oxidation in the $MnCo_2O_4$/FCNTs-PMS system has also been investigated. Fig. 4**C** shows the IBU degradation efficiency at different Cl^- concentrations. Different concentration levels of Cl^- from 1 to 10 mM were selected to simulate the actual wastewater concentration [29]. It can be noted that Cl^- performed a dual effect in the $MnCo_2O_4$/FCNTs-PMS system. With the increase of Cl^- concentration from 1 to 5 mM, the degradation efficiency of IBU decreased to 94.4% within 15 min. However, when the Cl^- concentration was further increased to 10 mM, IBU was degraded completely within less than 10 min. In the first 10 min, the k_{app} value for IBU removal gradually decreased from 0.285 to 0.135 min^{-1} with elevated Cl^- concentration from 0 to 2 mM, while it increased from 0.135 to 0.808 min^{-1} with further increased Cl^- concentration from 5 to 10 mM. The initial inhibition effect of Cl^- may result from the scavenging reaction between $SO_4^{\bullet-}$ and Cl^-. In the presence of Cl^-, secondary chlorine radicals (e.g., $Cl^{\bullet}$) with lower oxidation potentials were generated at the cost of undesired consumption of $SO_4^{\bullet-}$ in Eq. (4) [43]. When Cl^- concentration was higher than 5 mM, excessive $Cl^{\bullet}$ was generated along with the formation of Cl_2 and HOCl with $Cl^{\bullet}$ in the solution. The generated Cl_2 and HOCl were active to react with HSO_5^- via electron transfer to improve the catalytic activity of $MnCo_2O_4$/FCNTs-PMS system (Eqs. (1) - (4)), contributing to the IBU degradation [44,45].

$$Cl^- + HSO_5^- \rightarrow SO_4^{2-} + HOCl \quad (1)$$

$$Cl^- + {}^{\bullet}OH \rightarrow Cl^{\bullet} + OH^- \quad (2)$$

$$2Cl^- + H^+ + HSO_5^- \rightarrow SO_5^- + Cl_2 + H_2O \quad (3)$$

$$SO_4^{\bullet-} + Cl^- \rightarrow Cl^{\bullet} + SO_4^{2-} \quad (4)$$

3.3.4. Effect of HCO_3^-

The degradation of IBU by the $MnCo_2O_4$/FCNTs-PMS system in the presence of HCO_3^- has been examined and presented in Fig. 4D. Because higher concentration of HCO_3^- above 5 mM was reported to significantly inhibit the degradation of IBU [29], lower HCO_3^- concentration ranging 1–3 mM was investigated. It was observed that the k_{app} value for IBU decreased remarkably from 0.285 to 0.125 min^{-1} with the increasing HCO_3^- concentration from 1 m to 3 mM, indicating that HCO_3^- could inhibit IBU degradation. The presence of HCO_3^- could act as $SO_4^{\bullet-}$ and $^{\bullet}OH$ scavengers via Eqs. (5) and (6) [46] and the resulting carbonate radicals (i.e., $HCO_3^{\bullet}$ and $CO_3^{\bullet-}$) possessed lower redox potentials than either $SO_4^{\bullet-}$ or $^{\bullet}OH$.

$$SO_4^{\bullet-} + HCO_3^- \rightarrow SO_4^{2-} + HCO_3^{\bullet} \quad (5)$$

$$^{\bullet}OH + HCO_3^- \rightarrow OH^- + HCO_3^{\bullet} \quad (6)$$

3.3.5. Effect of NOM

Fig. 4E presents the effect of NOM on IBU removal in the $MnCo_2O_4$/FCNTs-PMS system. NOM can undergo competitive reaction with the generated ROS, leading to the decreasing decomposition efficiency towards IBU [9]. As shown in Fig. 4E, the presence of NOM significantly inhibited the degradation of IBU. For instance, the values of k_{app} for IBU was decreased from 0.285 to 0.092 min^{-1} as the NOM concentration was increased from 1 to 5 mg/L. Previous studies have also reported that reactions of target compounds with $SO_4^{\bullet-}$ and $^{\bullet}OH$ were slowed down by NOM, which was primarily due to its competitive consumption for oxidants as well as the low reactivity of resulting organic radicals [47–49]. Latest studies have revealed that NOM could undergo competitive reactions with $SO_4^{\bullet-}$ and $^{\bullet}OH$ and thus minimize the decomposition efficiency towards target components in AOPs, and its steric and electrostatic effects [32,50].

3.4. Stability and reusability of $MnCo_2O_4$/FCNTs

The stability and reusability of the catalyst is crucial for practical application. To evaluate the catalytic stability of $MnCo_2O_4$/FCNTs in the PMS oxidation system, the IBU removal study was conducted by using recycled catalyst over four cycles under identical reaction condition, and the results are shown in Fig. 4**F**. Apparently, it was found that IBU was still completely removed within 40 min after four cycles despite a slight decrease of k_{app} from 0.285 min^{-1} in the first cycle to 0.201 min^{-1} in the fourth cycle due to the loss of catalyst during catalyst recovery process. Moreover, the leaching concentrations of metal ions (i.e., Mn and Co) were below the detection limit of ICP-OES (1 μg/L), which were far lower than those reported in previous studies (i.e., 0.07–0.12 mg/L [51] up to 0.54–0.61 mg/L [52]). This indicates that the $MnCo_2O_4$/FCNTs was stable and its high activity could be maintained for at least four cycles.

The surface characteristics of $MnCo_2O_4$/FCNTs before and after catalytic reaction were measured by XPS. According to the high-resolution XPS spectra of Mn 2p depicted in Fig. 1, the Mn 2p profile of spent $MnCo_2O_4$ catalyst showed two main peaks at 642.2 eV and 643.2 eV which corresponded to Mn 2p3/2 and Mn 2p1/2, respectively. This implies that the Mn^{2+} chemical state on the sample surface [53,54] and the valence of Mn on the surface of spent catalyst had a noticeable change. Co 2p spectra exhibited two main peaks at binding energy of 781.2 and 796.1 eV which could be assigned to Co $2p_{3/2}$ and Co $2p_{1/2}$, respectively [55]. In addition, two satellite peaks confirmed the presence of Co^{3+} cation. These values were slightly shifted, and the area of peaks was decreased after the reaction with PMS and IBU, which suggested that Mn and Co species on the spent catalyst surface were in a mixed valence state. This suggests that Mn(II) and Co(III) on surface of the spent catalyst were partially transformed to Mn(III) and Co(II), respectively, during catalysis. Thus, it is proved that activation of PMS by $MnCo_2O_4$/FCNTs involved both redox pairs of Mn(II)/Mn(III) and Co(III)/Co(II) species therein, resulting in a higher catalytic activity.

3.5. Identification of ROS

In general, various highly reactive ROS, namely sulfate radical ($SO_4^{\bullet-}$), hydroxy radical ($^{\bullet}OH$), superoxide radical ($O_2^{\bullet-}$) and singlet oxygen ($^1O_2$) can be generated through radical and nonradical pathways to

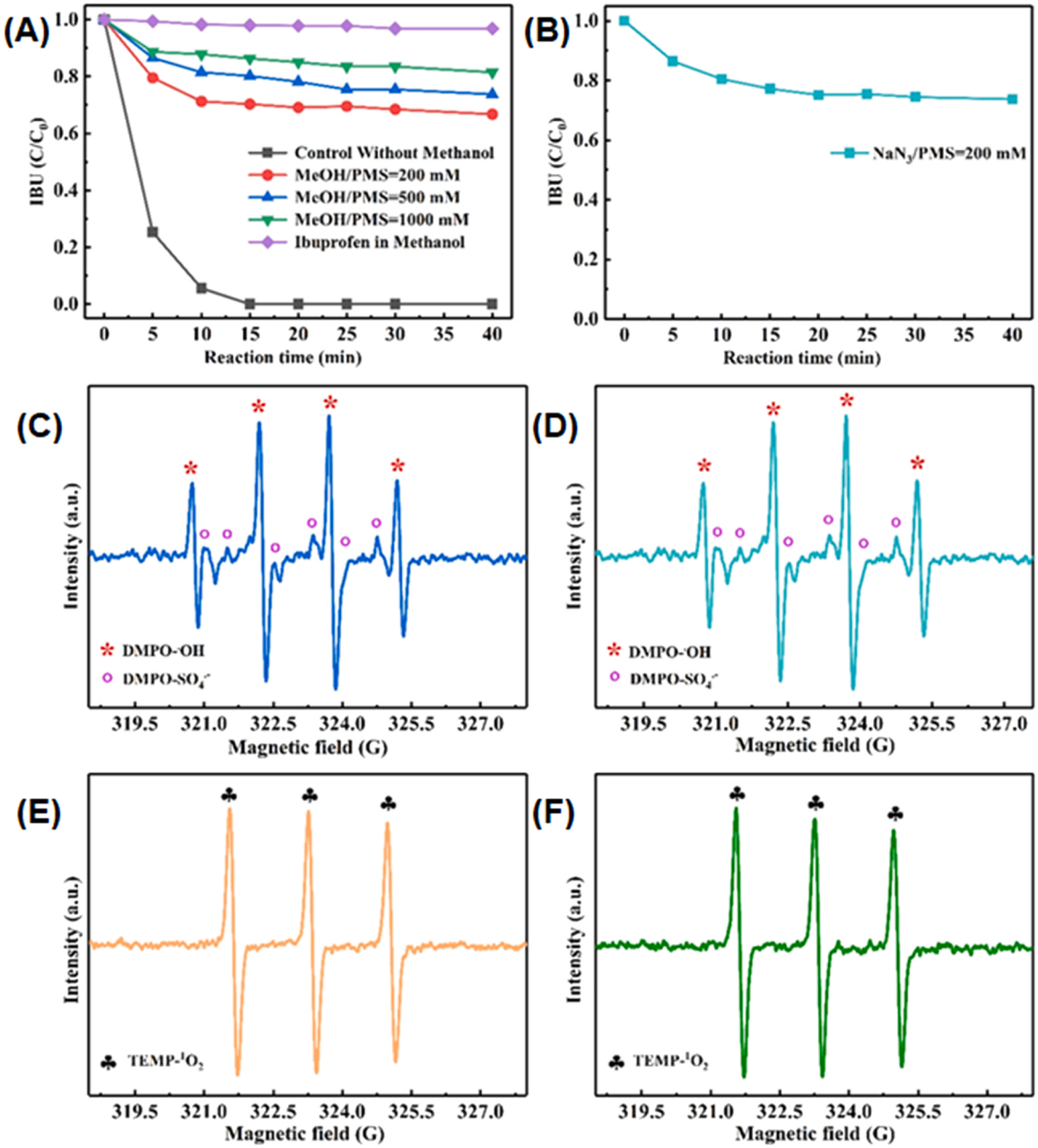

Fig. 5. (A – B) Effects of selected chemical scavengers on the IBU degradation, and EPR spectra of (C) and (D) for $MnCo_2O_4$/FCNTs-PMS system; (E) and (F) for FCNTs-PMS system) with DMPO or TEMP as the spin trapping agents.

degrade target pollutants. The radical pathway can be induced by redox reaction between PMS with both $MnCo_2O_4$ and FCNTs while the non-radical pathway can occur over FCNTs through the formation of surface activated PMS, direct electron transfer, formation of surface bound radicals, and singlet oxygen generation. To further confirm the dominant ROS for IBU degradation, quenching studies were carried out using MeOH and NaN_3 for radicals (e.g., $SO_4^{\bullet-}$, $^{\bullet}OH$ and $O_2^{\bullet-}$) and $^1O_2$, respectively. MeOH can quench both $SO_4^{\bullet-}$ and $^{\bullet}OH$ with high reaction rates ($k_{SO_4^{\bullet-}+MeOH}$= (1.6–7.7)× 10^7 $M^{-1}s^{-1}$, $k_{HO^{\bullet}+MeOH}$= (1.2–2.8)× 10^9 $M^{-1}s^{-1}$) [56], while it moderately reacts with $O_2^{\bullet-}$ at $k_{O_2^{\bullet-}+MeOH}$ of 1.5 × 10^8 M^{-1} s^{-1}. As shown in Fig. 5A, MeOH significantly affected the IBU removal in the $MnCo_2O_4$/FCNTs-PMS system. Upon addition of 200 mM MeOH, the IBU removal rate was partially inhibited by 84%. When the MeOH was increased to 1000 mM, the IBU removal was completely inhibited (>95%), indicating that MeOH had quenched most of the generated ROS, particularly $SO_4^{\bullet-}$, $^{\bullet}OH$ and $O_2^{\bullet-}$. Similarly, the addition of NaN_3 also resulted in a partial inhibition of IBU removal rate in Fig. 5B with a drastically decreased k_{app} of 0.035 min^{-1}, implying that $^1O_2$ could also be involved in the reaction system. These results indicate that both radical and nonradical pathways were involved in the catalytic degradation of IBU.

To further confirm the generation and effect of ROS in $MnCo_2O_4$/FCNTs-PMS system, EPR analysis was conducted using DMPO and TEMP as the spin trapping agents for radicals and $^1O_2$, respectively. For comparison, the FCNTs-PMS system was also studied using EPR. As illustrated in Fig. 5C and D, in the presence of PMS and DMPO, the signals of DMPO-$SO_4^{\bullet-}$ and DMPO-$^{\bullet}OH$ were clearly observed. Similarly, the signal corresponding to TEMP-$^1O_2$ was also observed when TEMP was used as the spin trapping agent. The peak intensities for the DMPO- $SO_4^{\bullet-}$ and DMPO-$^{\bullet}OH$ adducts in the $MnCo_2O_4$/FCNTs-PMS system were significantly higher than those for FCNTs-PMS, implying that the system had higher $SO_4^{\bullet-}$ and $^{\bullet}OH$ concentrations. Meanwhile, the intensity of

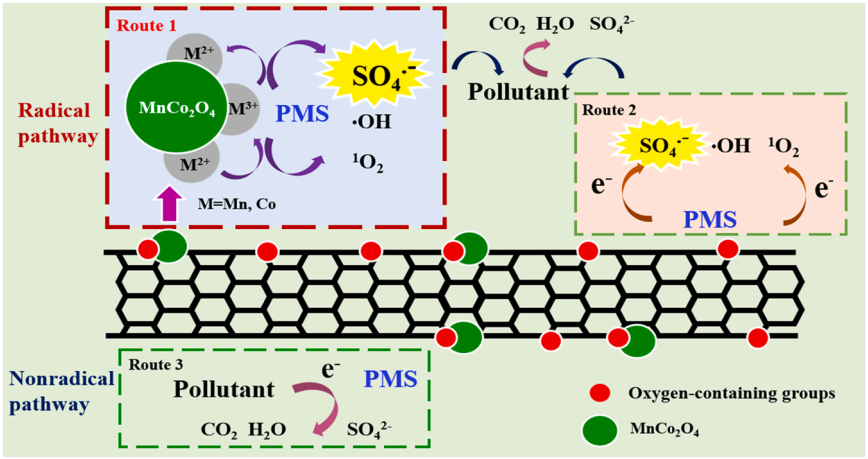

Fig. 6. Proposed PMS activation mechanism by $MnCo_2O_4$/FCNTs.

TEMP-$^1O_2$ for $MnCo_2O_4$/FCNTs-PMS and FCNTs-PMS was comparable. This confirms the existence of $SO_4^{\bullet-}$, $^{\bullet}OH$ and $^1O_2$, and providing conclusive evidence that the $SO_4^{\bullet-}$ and $^{\bullet}OH$ were generated at the $MnCo_2O_4$ active sites while the $^1O_2$ generation was produced at the FCNTs active sites.

3.6. Reaction mechanism

Based on acquired data and aforementioned discussion, a rational heterogeneous PMS activation mechanism by $MnCo_2O_4$/FCNTs is proposed in Fig. 6. It is speculated that the $MnCo_2O_4$ and FCNTs contributed to the production of $SO_4^{\bullet-}$ and $^{\bullet}OH$ (radical pathway), and $^1O_2$ (nonradical pathway), respectively. In general, transition metal-based catalysts are prone to activate PMS via the radical pathway while carbon-based catalysts can activate PMS through both radical and nonradical pathways. In the radical pathway, ≡Mn and ≡Co would react with surface hydroxyl groups (-OH) through dissociative adsorption of water molecules on $Co_xMn_{3-x}O_4$ surface to form ≡Mn(II) - ^-OH and ≡Co(II) - ^-OH, which could alter the oxidation state of the surface metal and offer active sites for further PMS activation [21]. Subsequently, the ≡Mn(II) - ^-OH species on $MnCo_2O_4$ surface can activate PMS to produce highly diffusible $SO_4^{\bullet-}$ in Eq. (7) and some more ≡Mn(II) - ^-OH species can be generated from the reaction of formed ≡Mn(III) - ^-OH species with PMS in Eq. (8). Similarly, ≡Co(II) - ^-OH species on the catalyst surface can also react with PMS to produce $SO_4^{\bullet-}$ in Eq. (9) and then more species are generated by the reactions between the formed ≡Co(III) - ^-OH species and PMS in Eq. (10). Since the reduction of ≡Co(III) by ≡Mn(II) in Eq. (11) was thermodynamically favorable [21], the formed ≡Mn(II) in Eq. (8) could further regenerate more ≡Co(II) species on the surface of $MnCo_2O_4$ to form more $SO_4^{\bullet-}$ via Eq. (9). Besides, as evidenced by XPS, ≡Mn(II)/≡Mn(III) and ≡Co(II)/≡Co(III) are redox couples that can react with PMS to generate $SO_4^{\bullet-}$ for oxidative degradation of IBU. Hence, there are more active sites on the catalyst, which further contributed to the catalytic activity of $MnCo_2O_4$/FCNTs. The cyclical regeneration of the catalyst occurred until PMS was completely consumed.

In the nonradical pathway, either the formation of surface activated complex or $^1O_2$ generation via PMS activation could occur. Regardless of either route, the PMS is firstly bonded with the sp^2-hybridized active sites of FCNTs. In the first scenario, the highly covalent π electrons could activate the O−O bond in PMS, leading to the production of $^1O_2$ for IBU degradation via Eq. (12) similar as $SO_4^{\bullet-}$ and $^{\bullet}OH$. In the second scenario, the adsorbed PMS is activated on the catalyst surface through forming outer-sphere complexes between FCNTs and PMS to facilitate the degradation of adsorbed IBU in Eq. (13). Nevertheless, the quantitative contribution of IBU degradation by radical and non-free radical pathways requires further investigations.

$$\equiv Mn(II) - {}^-OH + HSO_5^- \rightarrow \equiv Mn(III) - {}^-OH + SO_4^{\bullet-} + OH^- \quad (7)$$

$$\equiv Mn(III) - {}^-OH + HSO_5^- \rightarrow \equiv Mn(II) - {}^-OH + SO_5^{\bullet-} + H^+ \quad (8)$$

$$\equiv Co(II) - {}^-OH + HSO_5^- \rightarrow \equiv Co(III) - {}^-OH + SO_4^{\bullet-} + OH^- \quad (9)$$

$$\equiv Co(III) - {}^-OH + HSO_5^- \rightarrow \equiv Co(II) - {}^-OH + SO_5^{\bullet-} + H^+ \quad (10)$$

$$\equiv Mn(II) + Co(III) \rightarrow \equiv Mn(III) + Co(II),\ \Delta E = 0.30\ V \quad (11)$$

$$SO_4^{\bullet-} / {}^{\bullet}OH / {}^1O_2 + IBU \rightarrow [\ldots many\ steps \ldots] \rightarrow CO_2 + H_2O \quad (12)$$

$$IBU + surface\ activated\ PMS \rightarrow intermediates \rightarrow CO_2 + H_2O\ (nonradical) \quad (13)$$

4. Conclusions

This study has investigated the application of as-synthesized $MnCo_2O_4$/FCNTs as PMS activator for IBU degradation. Specifically, $MnCo_2O_4$ was uniformly decorated on FCNTs via a facile hydrothermal method and $MnCo_2O_4$/FCNTs was characterized using multi-scale techniques. In PMS system, $MnCo_2O_4$/FCNTs demonstrated excellent catalytic activity with k_{app} ranging 0.285–0.327 min^{-1} under a wide pH range of 3–9 within 10 min, achieving a complete removal of IBU and a mineralization rate higher than 90%. Moreover, $MnCo_2O_4$/FCNTs can be recycled for stable PMS activation with slight decrease of k_{app} from 0.285 to 0.201 min^{-1} after four cycles during the stability and reusability test. In addition, this catalyst was durable with negligible leaching of metal ions in the solution and could be promising eco-friendly PMS activator for highly efficient catalytic removal of organic pollutants. Furthermore, both radical and nonradical reactions are responsible for enhanced IBU degradation. $MnCo_2O_4$ and FCNTs contributed to the production of $SO_4^{\bullet-}$ and $^{\bullet}OH$ (radical pathway), and $^1O_2$ (nonradical pathway), respectively.

CRediT authorship contribution statement

Chao He: Conceptualization, Writing – review & editing, Supervision, Project administration, Funding acquisition. **Chunyan Tang:** Investigation, Writing – original draft. **Wen-Da Oh:** Data curation, Writing – review & editing.

Declaration of Competing Interest

The authors declare that they have no known competing financial

interests or personal relationships that could have appeared to influence the work reported in this paper.

Acknowledgements

C.H. thanks the financial support from National Natural Science Foundation of China (No. 51906264). J. Luo is acknowledged for the assistance of some experimental tests.

Appendix A. Supporting information

Supplementary data associated with this article can be found in the online version at doi:10.1016/j.jece.2022.107874.

References

[1] A.G. Katsikaros, C.V. Chrysikopoulos, Occurrence and distribution of pharmaceuticals and personal care products (PPCPs) detected in lakes around the world - a review, Environ. Adv. 6 (2021), 100131.
[2] R. Ricky, S. Shanthakumar, Phycoremediation integrated approach for the removal of pharmaceuticals and personal care products from wastewater – a review, J. Environ. Manag. 302 (2022), 113998.
[3] R. Yin, J. Sun, Y. Xiang, C. Shang, Recycling and reuse of rusted iron particles containing core-shell Fe-FeOOH for ibuprofen removal: adsorption and persulfate-based advanced oxidation, J. Clean. Prod. 178 (2018) 441–448.
[4] Y. Luo, W. Guo, H.H. Ngo, L.D. Nghiem, F.I. Hai, J. Zhang, S. Liang, X.C. Wang, A review on the occurrence of micropollutants in the aquatic environment and their fate and removal during wastewater treatment, Sci. Total Environ. 473–474 (2014) 619–641.
[5] C. Miege, J.M. Choubert, L. Ribeiro, M. Eusebe, M. Coquery, Fate of pharmaceuticals and personal care products in wastewater treatment plants-conception of a database and first results, Environ. Pollut. 157 (2009) 1721–1726.
[6] S. Wacławek, H.V. Lutze, K. Grübel, V.V.T. Padil, M. Černík, D.D. Dionysiou, Chemistry of persulfates in water and wastewater treatment: a review, Chem. Eng. J. 330 (2017) 44–62.
[7] P.-L. Koo, N.F. Jaafar, P.-S. Yap, W.-D. Oh, A review on the application of perovskite as peroxymonosulfate activator for organic pollutants removal, J. Environ. Chem. Eng. 10 (2022), 107093.
[8] H.V. Lutze, S. Bircher, I. Rapp, N. Kerlin, R. Bakkour, M. Geisler, C. von Sonntag, T. C. Schmidt, Degradation of chlorotriazine pesticides by sulfate radicals and the influence of organic matter, Environ. Sci. Technol. 49 (2015) 1673–1680.
[9] P. Hu, M. Long, Cobalt-catalyzed sulfate radical-based advanced oxidation: a review on heterogeneous catalysts and applications, Appl. Catal. B: Environ. 181 (2016) 103–117.
[10] F. Ghanbari, M. Moradi, Application of peroxymonosulfate and its activation methods for degradation of environmental organic pollutants: review, Chem. Eng. J. 310 (2017) 41–62.
[11] J. Sun, T. Wu, Z. Liu, B. Shao, Q. Liang, Q. He, S. Luo, Y. Pan, C. Zhao, D. Huang, Peroxymonosulfate activation induced by spinel ferrite nanoparticles and their nanocomposites for organic pollutants removal: A review, J. Clean. Prod. (2022), 131143.
[12] P.R. Shukla, S. Wang, H. Sun, H.M. Ang, M. Tadé, Activated carbon supported cobalt catalysts for advanced oxidation of organic contaminants in aqueous solution, Appl. Catal. B: Environ. 100 (2010) 529–534.
[13] W.-D. Oh, Z. Dong, T.-T. Lim, Generation of sulfate radical through heterogeneous catalysis for organic contaminants removal: Current development, challenges and prospects, Appl. Catal. B: Environ. 194 (2016) 169–201.
[14] J. Deng, Y. Ge, C. Tan, H. Wang, Q. Li, S. Zhou, K. Zhang, Degradation of ciprofloxacin using α-MnO_2 activated peroxymonosulfate process: effect of water constituents, degradation intermediates and toxicity evaluation, Chem. Eng. J. 330 (2017) 1390–1400.
[15] J. Gu, P. Yin, Y. Chen, H. Zhu, R. Wang, A natural manganese ore as a heterogeneous catalyst to effectively activate peroxymonosulfate to oxidize organic pollutants, Chin. Chem. Lett. (2022).
[16] S. Zhu, P. Xiao, X. Wang, Y. Liu, X. Yi, H. Zhou, Efficient peroxymonosulfate (PMS) activation by visible-light-driven formation of polymorphic amorphous manganese oxides, J. Hazard. Mater. 427 (2022), 127938.
[17] Y. Yao, C. Xu, S. Yu, D. Zhang, S. Wang, Facile synthesis of Mn_3O_4–Reduced graphene oxide hybrids for catalytic decomposition of aqueous organics, Ind. Eng. Chem. Res. 52 (2013) 3637–3645.
[18] A. Khan, Z. Liao, Y. Liu, A. Jawad, J. Ifthikar, Z. Chen, Synergistic degradation of phenols using peroxymonosulfate activated by CuO-Co_3O_4@MnO_2 nanocatalyst, J. Hazard. Mater. 329 (2017) 262–271.
[19] Y. Du, W. Ma, P. Liu, B. Zou, J. Ma, Magnetic $CoFe_2O_4$ nanoparticles supported on titanate nanotubes ($CoFe_2O_4$/TNTs) as a novel heterogeneous catalyst for peroxymonosulfate activation and degradation of organic pollutants, J. Hazard. Mater. 308 (2016) 58–66.
[20] P. Shi, X. Wang, X. Zhou, Y. Min, J. Fan, W. Yao, Influence of calcination temperature on the catalytic performance of Co3O4/GO nanocomposites for Orange II degradation, RSC Adv. 5 (2015) 34125–34133.
[21] Y. Yao, Y. Cai, G. Wu, F. Wei, X. Li, H. Chen, S. Wang, Sulfate radicals induced from peroxymonosulfate by cobalt manganese oxides (CoxMn3−xO4) for Fenton-Like reaction in water, J. Hazard. Mater. 296 (2015) 128–137.
[22] Y. Yao, Y. Cai, F. Lu, F. Wei, X. Wang, S. Wang, Magnetic recoverable $MnFe_2O_4$ and $MnFe_2O_4$-graphene hybrid as heterogeneous catalysts of peroxymonosulfate activation for efficient degradation of aqueous organic pollutants, J. Hazard. Mater. 270 (2014) 61–70.
[23] X. Li, H. Lu, Y. Zhang, F. He, Efficient removal of organic pollutants from aqueous media using newly synthesized polypyrrole/CNTs-$CoFe_2O_4$ magnetic nanocomposites, Chem. Eng. J. 316 (2017) 893–902.
[24] S. Song, S. Jiang, Selective catalytic oxidation of ammonia to nitrogen over CuO/CNTs: the promoting effect of the defects of CNTs on the catalytic activity and selectivity, Appl. Catal. B: Environ. 117–118 (2012) 346–350.
[25] Y.N. Liang, W.-D. Oh, Y. Li, X. Hu, Nanocarbons as platforms for developing novel catalytic composites: overview and prospects, Appl. Catal. A: Gen. 562 (2018) 94–105.
[26] Q. Yang, H. Choi, S.R. Al-Abed, D.D. Dionysiou, Iron–cobalt mixed oxide nanocatalysts: Heterogeneous peroxymonosulfate activation, cobalt leaching, and ferromagnetic properties for environmental applications, Appl. Catal. B: Environ. 88 (2009) 462–469.
[27] C. He, J. Zheng, K. Wang, H. Lin, J.-Y. Wang, Y. Yang, Sorption enhanced aqueous phase reforming of glycerol for hydrogen production over Pt-Ni supported on multi-walled carbon nanotubes, Appl. Catal. B: Environ. 162 (2015) 401–411.
[28] A.B.A.A. Nassr, I. Sinev, W. Grünert, M. Bron, PtNi supported on oxygen functionalized carbon nanotubes: In depth structural characterization and activity for methanol electrooxidation, Appl. Catal. B: Environ. 142–143 (2013) 849–860.
[29] Z. Ren, H. Romar, T. Varila, X. Xu, Z. Wang, M. Sillanpää, T. Leiviskä, Ibuprofen degradation using a Co-doped carbon matrix derived from peat as a peroxymonosulphate activator, Environ. Res. 193 (2021), 110564.
[30] Z. Guo, Y. Chen, L. Li, X. Wang, G.L. Haller, Y. Yang, Carbon nanotube-supported Pt-based bimetallic catalysts prepared by a microwave-assisted polyol reduction method and their catalytic applications in the selective hydrogenation, J. Catal. 276 (2010) 314–326.
[31] X. Chen, W.-D. Oh, Z.-T. Hu, Y.-M. Sun, R.D. Webster, S.-Z. Li, T.-T. Lim, Enhancing sulfacetamide degradation by peroxymonosulfate activation with N-doped graphene produced through delicately-controlled nitrogen functionalization via tweaking thermal annealing processes, Appl. Catal. B: Environ. 225 (2018) 243–257.
[32] C. Guan, J. Jiang, C. Luo, S. Pang, Y. Yang, Z. Wang, J. Ma, J. Yu, X. Zhao, Oxidation of bromophenols by carbon nanotube activated peroxymonosulfate (PMS) and formation of brominated products: Comparison to peroxydisulfate (PDS), Chem. Eng. J. 337 (2018) 40–50.
[33] C. Shen, Y. Wang, J. Fu, Urchin-like Co3O4 anchored on reduced graphene oxide with enhanced performance for peroxymonosulfate activation in ibuprofen degradation, J. Environ. Manag. 307 (2022), 114572.
[34] M. Naderi, R. Darvishi, Cheshmeh Soltani, Hybrid of ZnFe layered double hydroxide/nano-scale carbon for activation of peroxymonosulfate to decompose ibuprofen: Thermodynamic and reaction pathways investigation, Environ. Technol. Innov. 24 (2021), 101951.
[35] A. Naima, F. Ammar, O. Abdelkader, C. Rachid, H. Lynda, A. Syafiuddin, R. Boopathy, Development of a novel and efficient biochar produced from pepper stem for effective ibuprofen removal, Bioresour. Technol. 347 (2022), 126685.
[36] S.K. Rani, D. Easwaramoorthy, I.M. Bilal, M. Palanichamy, Studies on Mn(II)-catalyzed oxidation of α-amino acids by peroxomonosulphate in alkaline medium-deamination and decarboxylation: A kinetic approach, Appl. Catal. A: Gen. 369 (2009) 1–7.
[37] M.A. Atieh, O.Y. Bakather, B. Al-Tawbini, A.A. Bukhari, F.A. Abuilaiwi, M. B. Fettouhi, Effect of carboxylic functional group functionalized on carbon nanotubes surface on the removal of lead from water, Bioinorg. Chem. Appl. 2010 (2010), 603978.
[38] J. Cui, T. Liu, Q. Zhang, T. Wang, X. Hou, Rapid microwave synthesis of Fe3O4-PVP@ ZIF-67 as highly effective peroxymonosulfate catalyst for degradation of bisphenol F and its mechanism analysis, Chem. Eng. J. 404 (2021), 126453.
[39] J. Liang, M. Guo, Y. Xue, J.-n Gu, J. Li, F. Shi, X. Guo, X. Min, J. Jia, K. Li, T. Sun, Constructing magnetically separable manganese-based spinel ferrite from spent ternary lithium-ion batteries for efficient degradation of bisphenol A via peroxymonosulfate activation, Chem. Eng. J. 435 (2022), 135000.
[40] E. Saputra, J.A. Pinem, M.A. Budihardjo, P.S. Utama, S. Wang, Carbon-supported manganese for heterogeneous activation of peroxymonosulfate for the decomposition of phenol in aqueous solutions, Mater. Today Chem. 16 (2020), 100268.
[41] X. Duan, S. Indrawirawan, J. Kang, W. Tian, H. Zhang, H. Sun, S. Wang, Temperature-dependent evolution of hydroxyl radicals from peroxymonosulfate activation over nitrogen-modified carbon nanotubes, Sustain. Mater. Technol. 18 (2018).
[42] X. Huang, X. Zhou, J. Zhou, Z. Huang, S. Liu, G. Qian, N. Gao, Bromate inhibition by reduced graphene oxide in thermal/PMS process, Water Res. 122 (2017) 701–707.
[43] R. Yuan, S.N. Ramjaun, Z. Wang, J. Liu, Effects of chloride ion on degradation of Acid Orange 7 by sulfate radical-based advanced oxidation process: implications for formation of chlorinated aromatic compounds, J. Hazard Mater. 196 (2011) 173–179.
[44] G.P. Anipsitakis, T.P. Tufano, D.D. Dionysiou, Chemical and microbial decontamination of pool water using activated potassium peroxymonosulfate, Water Res. 42 (2008) 2899–2910.

[45] C. Liang, Z.S. Wang, N. Mohanty, Influences of carbonate and chloride ions on persulfate oxidation of trichloroethylene at 20 degrees C, Sci. Total. Environ. 370 (2006) 271–277.
[46] J.-C.E. Yang, B. Yuan, H.-J. Cui, S. Wang, M.-L. Fu, Modulating oxone-MnOx/silica catalytic systems towards ibuprofen degradation: Insights into system effects, reaction kinetics and mechanisms, Appl. Catal. B: Environ. 205 (2017) 327–339.
[47] C. Luo, J. Jiang, J. Ma, S. Pang, Y. Liu, Y. Song, C. Guan, J. Li, Y. Jin, D. Wu, Oxidation of the odorous compound 2,4,6-trichloroanisole by UV activated persulfate: Kinetics, products, and pathways, Water Res. 96 (2016) 12–21.
[48] S. Yang, T. Xiao, J. Zhang, Y. Chen, L. Li, Activated carbon fiber as heterogeneous catalyst of peroxymonosulfate activation for efficient degradation of Acid Orange 7 in aqueous solution, Sep. Purrif. Technol. 143 (2015) 19–26.
[49] Y.H. Guan, J. Ma, Y.M. Ren, Y.L. Liu, J.Y. Xiao, L.Q. Lin, C. Zhang, Efficient degradation of atrazine by magnetic porous copper ferrite catalyzed peroxymonosulfate oxidation via the formation of hydroxyl and sulfate radicals, Water Res. 47 (2013) 5431–5438.
[50] C. Guan, J. Jiang, C. Luo, S. Pang, C. Jiang, J. Ma, Y. Jin, J. Li, Transformation of iodide by carbon nanotube activated peroxydisulfate and formation of iodoorganic compounds in the presence of natural organic matter, Environ. Sci. Technol. 51 (2017) 479–487.
[51] J. Lu, Q. Liu, Z. Xiong, Z. Xu, Y. Cai, Q. Wang, Activation of peroxymonosulfate with magnetic and recyclable Fe3O4@C/MnCo2O4 nanocomposites for the decolorization of Acid Orange II, J. Chem. Technol. Biotechnol. 92 (2017) 1601–1612.
[52] Q. Wang, Z. Xu, Y. Jiang, J. Lu, H. Li, X. Du, Z. Wang, Efficient peroxymonosulfate activation and less metallic leaching through kaolin@MnCo2O4 for bisphenol A degradation in environmental remediation, Appl. Surf. Sci. 585 (2022), 152705.
[53] Y. Yao, Y. Cai, F. Lu, F. Wei, X. Wang, S. Wang, Magnetic recoverable $MnFe_{(2)}O_{(4)}$ and $MnFe_{(2)}O_{(4)}$-graphene hybrid as heterogeneous catalysts of peroxymonosulfate activation for efficient degradation of aqueous organic pollutants, J. Hazard. Mater. 270 (2014) 61–70.
[54] Y. Yao, Y. Cai, G. Wu, F. Wei, X. Li, H. Chen, S. Wang, Sulfate radicals induced from peroxymonosulfate by cobalt manganese oxides ($Co_{(x)}Mn_{(3-x)}O_4$) for Fenton-Like reaction in water, J. Hazard. Mater. 296 (2015) 128–137.
[55] Y. Feng, J. Liu, D. Wu, Z. Zhou, Y. Deng, T. Zhang, K. Shih, Efficient degradation of sulfamethazine with $CuCo_2O_4$ spinel nanocatalysts for peroxymonosulfate activation, Chem. Eng. J. 280 (2015) 514–524.
[56] S.-H. Ho, Y.-d Chen, R. Li, C. Zhang, Y. Ge, G. Cao, M. Ma, X. Duan, S. Wang, N.-q Ren, N-doped graphitic biochars from C-phycocyanin extracted Spirulina residue for catalytic persulfate activation toward nonradical disinfection and organic oxidation, Water Res. 159 (2019) 77–86.